Numerical Simulation of Temperature Distribution in Melt Spinning of PET Monofilament

Tae Hwan Oh

Huvis R&D Center, 1690–1, Shinil Dong, Daedeok Ku, Daejeon, South Korea

Received 13 November 2005; accepted 31 January 2006
DOI 10.1002/app.24197
Published online in Wiley InterScience (www.interscience.wiley.com).

ABSTRACT: Numerical simulation for calculating temperature distributions, including the axial and radial temperature gradients in the melt spinning of polyethylene terephthalate (PET) monofilament, was performed. The finite difference method was used to calculate the radial temperature distribution. Newtonian and the upper convected Maxwell models were adopted as a constitutive equation, respectively. There is little difference in the axial and radial temperature profiles between Newtonian and the upper convected Maxwell constitutive equations. The effect of spinning conditions on the temperature difference between the core and surface was investigated. Quench air velocity is the most effective process variable in controlling the temperature difference. Quench air velocity profiles were investigated to reduce the temperature difference between the core and surface. Lower quench air velocity profile at initial deformation zone leads to a decrease in temperature difference between the core and surface. © 2006 Wiley Periodicals, Inc. J Appl Polym Sci 102: 1045–1051, 2006

Key words: temperature distributions; radial and axial temperature gradients; upper convected Maxwell; temperature difference; quench air velocity profiles

INTRODUCTION

Melt spinning is a widely used method for manufacturing synthetic fibers. It was mainly analyzed by using an asymptotic method, which simplifies the governing equations to one-dimensional form.[1–3] The temperature gradient within a running filament in the melt spinning is important in determining the properties of fiber. The radial temperature gradient has to be considered for an accurate analysis in the spinning of thick monofilament. The temperature difference between surface and core leads to a viscosity difference and it affects the physical properties of resulting as-spun fibers. Most numerical calculations have been presented for calculating the axial temperature distribution along the spinline.[4–7] The temperature field in melt spinning is mainly determined by axial convection and radial conduction because of large length to diameter ratio, and thus many approaches focused on the consideration of forced convection.[8,9]

In this work, a mathematical model for calculating the radial temperature distribution of thick monofilament was presented and the effect of spinning conditions and quench air velocity profiles on temperature difference between the core and surface were investigated.

Correspondence to: T.H. Oh (ohth@huvis.com).

Journal of Applied Polymer Science, Vol. 102, 1045–1051 (2006)

FORMULATION AND NUMERICAL METHOD

A cylindrical coordinate system was employed for a numerical procedure. For steady, incompressible flow, the asymptotic equations averaged over cross section for conservation of mass, momentum, and energy are as follows:[5]

$$W = \rho A v_z \tag{1}$$

$$dF/dz = W(dv_z/dz - g/v_z) + \pi\rho v_z^2 C_f D/2 \tag{2}$$

$$dT/dz = -\pi Dh(T - T_a)/(WC_p) \tag{3}$$

where W represents the mass flow rate of polymer, A the area of fiber, v_z the axial velocity, ρ the density of polymer, F the force, z the position in axial direction, D the diameter, C_f the skin friction coefficient, g the gravity constant, C_p the specific heat capacity of polymer, h the heat transfer coefficient of polymer, T the temperature of polymer, and T_a the temperature of surrounding air. Here, Newtonian and viscoelastic fluid as constitutive equations were assumed, respectively. The constitutive equation of each fluid is presented as

Newtonian model:

$$F = \eta A(dv_z/dz) \tag{4}$$

where η is the elongational viscosity.

Upper convected Maxwell model:[6]

TABLE I
Material Parameters used in the Simulation

Parameters	Values
Thermal conductivity of air (k_a, g cm/(s °C))	2.63×10^3
Kinematic viscosity of air (μ_a, cm^2/s)	0.29
Thermal conductivity of PET (k_p, g cm/s^3 °C)	2.09×10^4
Specific heat capacity of PET (C_p, cm^2/s^2 °C)	$(0.3 + 6.0 \times 10^{-4}T) \times 4.2 \times 10^7$
Density of PET (ρ, g/cm^3)	$1.356 - 5 \times 10^{-4}T$

$$\sigma + \lambda[\partial\sigma/\partial t + \nu \cdot \nabla\sigma - (\nabla\nu) \cdot \sigma - \sigma \cdot (\nabla\nu)^{\mathrm{T}} - \sigma(\partial \ln T/\partial t) - \sigma \cdot (\nu\nabla \ln T)] = \mu[\nabla\nu + (\nabla\nu)^{\mathrm{T}}] \quad (5)$$

where σ is the total stress tensor, λ the relaxation time of polymer, ν the velocity vector, μ the shear viscosity, and t the time. In a steady state condition, eq. (5) can be written as a component form:

$$\tau_{zz} + \lambda[\nu_z(d\tau_{zz}/dz) - 2\tau_{zz}(d\nu_z/dz) - \nu_z\tau_{zz}(d \ln T/dz)] = 2\mu(d\nu_z/dz) \quad (6)$$

$$\tau_{rr} + \lambda[\nu_z(d\tau_{rr}/dz) - 2\tau_{rr}(d\nu_z/dz) - \nu_z\tau_{rr}(d \ln T/dz)] = \mu(d\nu_z/dz) \quad (7)$$

where τ_{zz} is the axial stress and τ_{rr} is the radial stress.

Equations (6) and (7) can be simplified to the following form:

$$\tau_{zz} - \tau_{rr} = F/A \quad (8)$$

$$d\tau_{zz}/dz = (2\tau_{zz}/\nu_z + 2\eta/3\lambda\nu_z)(d\nu_z/dz) - \tau_{zz}/\lambda\nu_z + \tau_{zz}(d \ln T/dz) \quad (9)$$

where $\tau_{zz} - \tau_{rr}$ is the total stress.

The elongational viscosity of polyethylene terephthalate (PET) was assumed to be only a function of temperature and expressed as follows:[10]

$$\eta = 0.73 \times \exp\left(\frac{5300}{T + 273}\right) \quad (10)$$

To derive above-mentioned equations, a purely extensional flow field was assumed and the viscous dissipation was neglected. The basic equations are strongly coupled with a lack of one more single equation for analytical calculation. Therefore a shooting method was used with initial guess of the force at the die (at $z = 0$) to fit the boundary condition of spinning speed. The boundary conditions applied in the simulation are expressed as:

$$T(0) = T_{\mathrm{die}}, \quad \nu_z(0) = \nu_0, \quad \nu_z(L) = \nu_L \quad (11)$$

where T_{die} is the spinning temperature, ν_0 the initial speed, ν_L the spinning speed, and L the distance from spinneret to solidification point defined as the point at which the temperature of the filament is equal to its glass transition temperature. The dimensions of spinnerets as the starting diameter in the simulation were used. Since the spinning process has a large length-to-diameter ratio, the die swell effect could be neglected. The fourth-order Runge–Kutta method was used to solve the asymptotic equations. Several correlations for physical properties and transport coefficients are expressed as below and some material parameters are summarized in Table I.[10–14]

$$h = 0.42\left(\frac{k_a}{D}\right)Re_d^{0.334}\left[1 + \left(\frac{8\nu_a}{\nu_z}\right)^2\right]^{0.1667} \quad (12)$$

$$C_f = 0.37Re_d^{-0.61} \quad (13)$$

$$Re_d = \left(\frac{\nu_z D}{\mu_a}\right) \quad (14)$$

where k_a is the thermal conductivity of air, ν_a the quench air velocity, μ_a the kinematic viscosity of air and Re_d the Reynolds number.

If the molten polymer is considered to be incompressible, then the continuity relation can be written as

$$\frac{1}{r}\frac{\partial}{\partial r}(r\nu_r) + \frac{\partial}{\partial z}\nu_z = 0 \quad (15)$$

where r is the radial position in radial direction and ν_r is the radial velocity. The energy equation describing the two-dimensional heat transfer in the melt spinning is written as[7]

$$\frac{WC_p}{\pi R^2}\left[\frac{r}{R}\frac{dR}{dz}\frac{\partial T}{\partial r} + \frac{\partial T}{\partial z}\right] = k_p\left[\frac{\partial^2 T}{\partial r^2} + \frac{1}{r}\frac{\partial T}{\partial r}\right] \quad (16)$$

where k_p is the thermal conductivity of polymer and R is the radius.

The dimensionless radial and axial coordinates are defined as follows:[7,8]

$$\xi = \frac{r}{R}, \quad \zeta = \frac{\pi k_p z}{WC_p}, \quad \theta = \frac{T - T_a}{T_{\text{die}} - T_a} \tag{17}$$

Then, eq. (16) can be simplified by expressing it in terms of dimensionless variables. The dimensionless form of energy equation is introduced as follows:

$$\frac{\partial \theta}{\partial \zeta} = \frac{\partial^2 \theta}{\partial \xi^2} + \frac{1}{\xi}\frac{\partial \theta}{\partial \xi} \tag{18}$$

The boundary conditions are as:[7]

$$T(r,0) = T_{\text{die}}; \quad \theta(\xi,0) = 1.0 \tag{19}$$

$$\frac{\partial T(0,z)}{\partial r} = 0; \quad \frac{\partial \theta(0,\zeta)}{\partial \xi} = 0 \tag{20}$$

$$\frac{\partial T(R,z)}{\partial r} = -\frac{h}{k_p}(T(R,z) - T_a); \quad \frac{\partial \theta(1,\zeta)}{\partial \xi} = -\frac{hR}{k_p}\theta \tag{21}$$

The implicit Crank–Nicolson method was used to solve the eq. (18). The finite difference equation of the eq. (18) for the grid points is given by

$$A_k\theta_{k-1,n+1} + B_k\theta_{k,n+1} + C_k\theta_{k-1,n+1} = D_k \tag{22}$$

where

$$A_k = k - \frac{3}{2},$$

$$B_k = -\frac{2(k-1)(\Delta\xi)^2}{\Delta\zeta} - 2(k-1),$$

$$C_k = k - \frac{1}{2},$$

$$D_k = \left[-k + \frac{3}{2}\right]\theta_{k-1,n} + \left[-\frac{2(k-1)(\Delta\xi)^2}{\Delta\zeta} + 2(k-1)\right]\theta_{k,n} + \left[-k + \frac{1}{2}\right]\theta_{k+1,n}$$

For the center grid point ($k = 1$), the finite difference equation is

$$B_1\theta_{1,n+1} + C_1\theta_{2,n+1} = D_1 \tag{23}$$

where

$$B_1 = -2 - \frac{2(\Delta\xi)^2}{\Delta\zeta}, \quad C_1 = 2,$$

$$D_1 = \left[2 - \frac{2(\Delta\xi)^2}{\Delta\zeta}\right]\theta_{1,n} + [-2]\theta_{2,n}$$

The finite difference equation for the surface grid point ($k = L$) is

$$A_L\theta_{L-1,n+1} + B_L\theta_{L,n+1} = D_L \tag{24}$$

where

$$A_L = 2,$$

$$B_L = -\frac{2(\Delta\xi)^2}{\Delta\zeta} - 2 - 2\left(\frac{hR}{k_p}\right)(\Delta\xi) - \left(\frac{hR}{k_p}\right)(\Delta\zeta)^2,$$

$$D_L = [-2]\theta_{L\,1,n} + \left[-\frac{2(\Delta\xi)^2}{\Delta\zeta} + 2 + 2\left(\frac{hR}{k_p}\right)(\Delta\xi) + \left(\frac{hR}{k_p}\right)(\Delta\xi)^2\right]\theta_{L,n}$$

The matrix of eq. (22) was solved using Gauss–Seidel iterative method. The conditions for a simulation chosen in this work are summarized in Table II.

EXPERIMEMTAL

Melt spinning

Fiber-forming polymeric material used in this work was a textile grade PET of which the intrinsic viscosity was 0.63 dL/g. A spinneret plate with 4 bores, bore diameter of 0.3 mm and length-to-diameter ratio of 2, was employed. To estimate the diameter of a running filament along the spinline, a fiber-capturing device was used. The shortest possible length was captured to prevent the sag of extrudate. The design of this apparatus originated from Kase's work,[15] in which he used it to cut a specific length of fiber from the running spinline and calculated the linear density of fiber. Also, Ishibashi et al.[16] used a similar apparatus to capture running filaments and determined fiber diameter.

RESULTS AND DISCUSSION

Figure 1 shows the diameter profile for calculated and experiment values. Numerical simulations fit experimental values well. Figures 2 and 3 show computed temperature profiles and temperature differences along the spinline. There exists a maximum in temperature differences between the core and surface near the spinneret and then the temperature difference decreases gently along the spinline. The maximum value

TABLE II
Conditions of Melt Spinning in the Simulation

No.	Mass flow rate (g/min hole)	Spinning temperature (°C)	Spinning speed (m/min)	Quench air velocity (m/s)	Quench air temperature (°C)	Linear density (dtex)
1	4.4	290	1500	0.3	20	29.33
2	4.0	290	1500	0.3	20	26.67
3	3.6	290	1500	0.3	20	24.00
4	3.2	290	1500	0.3	20	21.33
5	2.8	290	1500	0.3	20	18.67
6	4.0	290	1300	0.3	20	30.80
7	4.0	290	1400	0.3	20	28.57
8	4.0	290	1600	0.3	20	25.00
9	4.0	290	1700	0.3	20	23.53
10	4.0	290	1500	0.2	20	26.67
11	4.0	290	1500	0.4	20	26.67
12	4.0	290	1500	0.5	20	26.67
13	4.0	290	1500	0.6	20	26.67
14	4.0	290	1500	0.3	22	26.67
15	4.0	290	1500	0.3	24	26.67
16	4.0	290	1500	0.3	26	26.67
17	4.0	290	1500	0.3	28	26.67
18	4.0	280	1500	0.3	20	26.67
19	4.0	282.5	1500	0.3	20	26.67
20	4.0	285	1500	0.3	20	26.67
21	4.0	287.5	1500	0.3	20	26.67

of temperature difference is 10.9°C at $z = 4.3$ cm. Temperature difference at the onset of solidification of PET is 2.5°C at $z = 158$ cm. There is little difference between Newtonian and upper convected Maxwell models, i.e., the temperature profiles are mainly dependent on process conditions not rheological characteristics of fluid. The former research[14] showed that only using Newtonian constitutive equation fits the dynamics of melt spinning process except for the analysis of instability problem. Figure 4 shows the radial temperature distributions for different axial positions. The radial temperature profiles are bent [Fig. 4(a)] at initial deformation zone due to a large temperature difference and flatten near the solidification point [Fig. 4(b)].

The effects of process conditions on the maximum temperature difference are shown in Figure 5. Here,

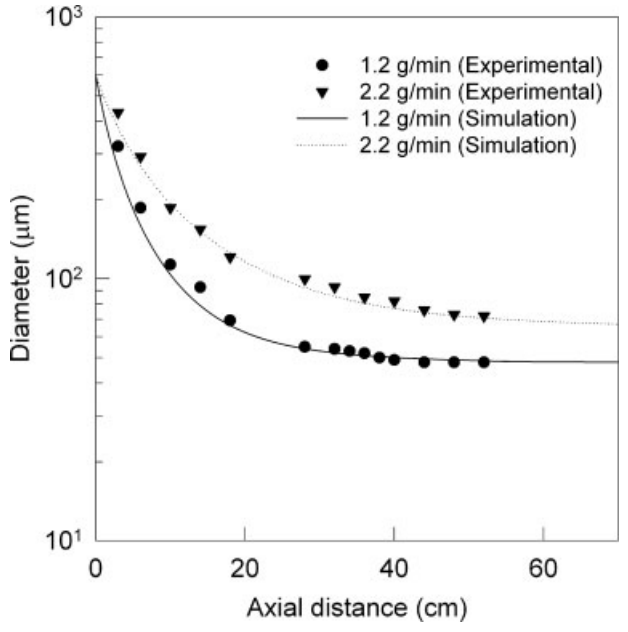

Figure 1 Comparison of computed and experimental diameter profiles along the spinline: spinning temperature, 290°C; take-up speed, 500 m/min; quench air velocity, 0.3 m/s; quench air temperature, 24°C.

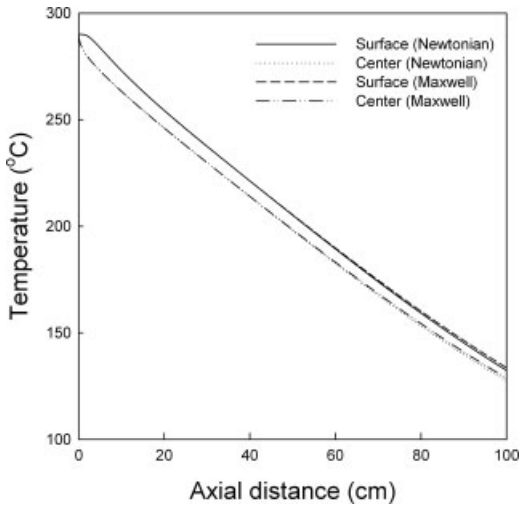

Figure 2 Computed center and surface temperature profiles along the spinline: simulation condition, No. 2.

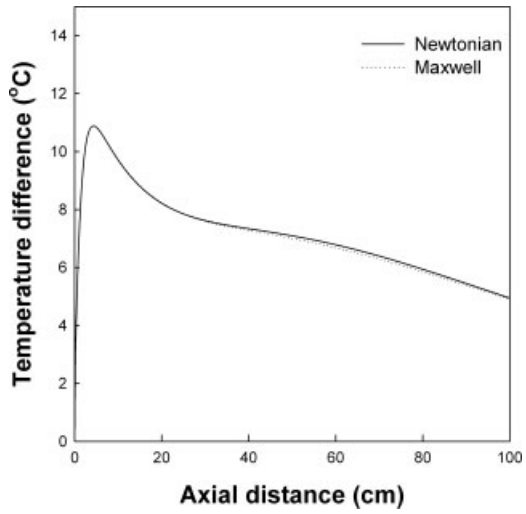

Figure 3 Temperature difference profiles between the center and surface along the spinline: simulation condition, No. 2.

ΔT_{max} means the maximum temperature difference between the core and surface of running filament along the spinline. Each mean value of given spinning conditions was calculated and the differences were nondimensionalized,[12] and the percent change of spinning conditions from mean value was obtained. As shown in Figure 5, a quench air velocity has more significant effect than the other process conditions on the ΔT_{max}. The ΔT_{max} changes from 8.9°C to 12.2°C with the quench air velocity and ranges from 9.5°C to 10.0°C for the other process conditions. Since PET possesses a high melt flow index in comparison with the other polymers, the control of quenching conditions is necessary for solidification in forced convection. Quench blown air controls the position of the freezing point, which is an important factor for the stability of the spinline. Except for quench air velocity, the temperature difference changes little with spinning conditions. Quench air temperature is another quenching variable but it has little effect on the ΔT_{max}. Quenching efficiency depends mainly on the heat transfer by forced convection determined by the temperature difference between filament and surrounding air, i.e., supercooling [eq. (3)]. However, the difference between the temperature of molten polymer and surrounding air is so large as to neglect the variation of quench air temperature so the quench air temperature has little effect on ΔT_{max}. Axial position at maximum temperature difference ($Z_{\Delta T_{max}}$) is mainly affected by mass flow rate (Fig. 6). As shown in Figure 5, the mass flow rate has little effect on the ΔT_{max}. However, as the mass flow rate increases, the $Z_{\Delta T_{max}}$ moves downward from the spinneret. In general, a higher mass flow rate lengthens the solidification point and needs more efficient cooling conditions for solidification. As the mass flow rate decreases, the initial velocity decreased and thus drawdown ratio increased and the diameter at initial deformation region decreased swiftly. This leads to a higher heat transfer to an ambient air and thus $Z_{\Delta T_{max}}$ moves upward. Take-up speed, quench air temperature, and spinning temperature have smaller effect on the $Z_{\Delta T_{max}}$. The $Z_{\Delta T_{max}}$ moves upward smoothly with increasing quench air velocity.

The control of quench air velocity profiles along the axial direction is difficult with a normal quenching apparatus. However, to find the way to reduce the ΔT_{max}, some quench air velocity profiles were assumed and the temperature profiles were calculated using them. Figure 7 shows the schematic of assumed

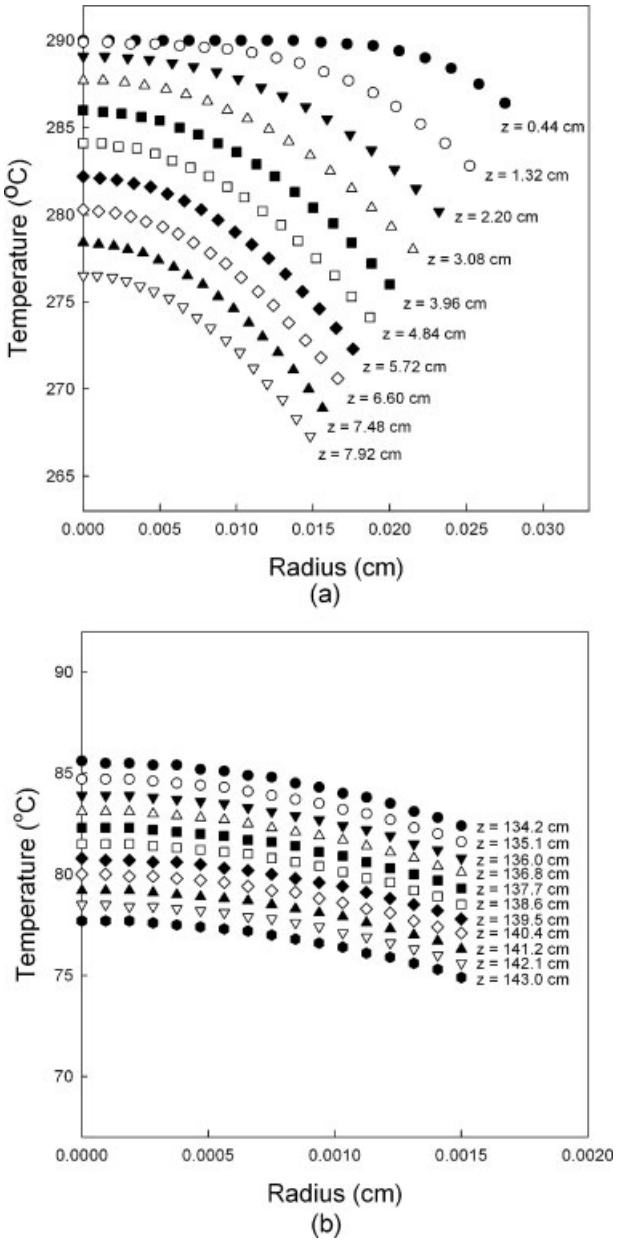

Figure 4 Radial temperature distributions (a) at initial deformation region and (b) near solidification region: simulation condition, No. 2.

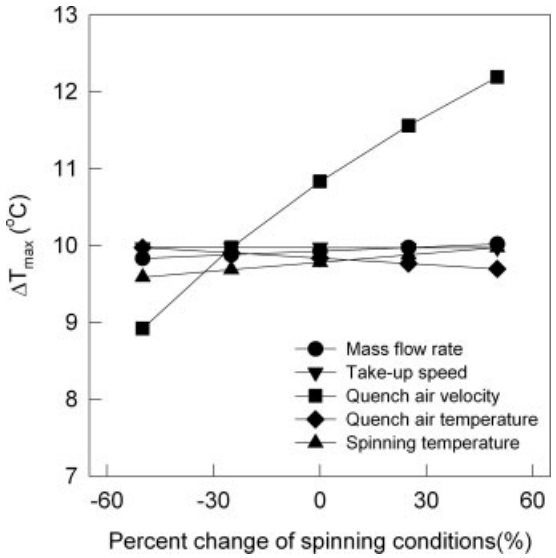

Figure 5 Maximum temperature difference versus percent change of spinning conditions.

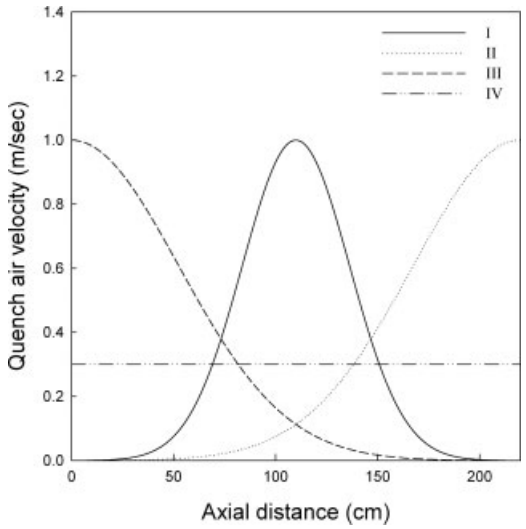

Figure 7 Schematics of assumed quench air profiles.

quench air velocity profiles. There are one Gaussian distribution (I), two skewed distributions (II and III), and the other normal side quenching (IV). All quench air velocity profiles were assumed to have the same quantity of quench air. Figure 8 is a plot of the ΔT_{max} versus types of quench air velocity profile. The type I and II have the least ΔT_{max}. The ΔT_{max} reduces from 10.8°C for normal side quenching to 7.6°C for the skewed and Gaussian distributions. Higher quench air velocity at initial deformation zone (type III) induces the increased ΔT_{max} up to 15.4°C. The lower quench air velocity at initial deformation zone is necessary for the lower ΔT_{max}.

CONCLUSIONS

To analyze the effect of spinning conditions on temperature distribution in the radial and axial directions, the numerical simulations were performed. Temperature distributions, including the radial and axial temperature gradient during the melt spinning of PET were calculated. The temperature difference between the core and surface did not depend on the constitutive equations. The maximum temperature differences between the core and surface range from 9.0°C to 10°C for all spinning conditions except for quench air velocity. Quench air velocity is the most effective variable in controlling the radial temperature distribution and the mass flow rate has the effect on axial position of maximum temperature difference. Lower quench

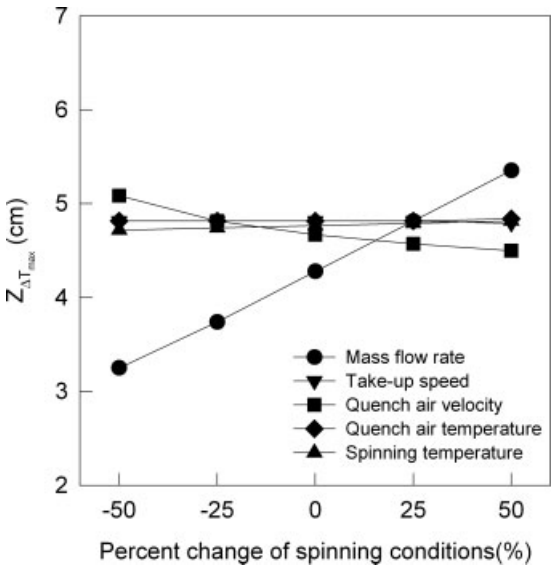

Figure 6 Axial position at maximum temperature difference versus percent change of spinning conditions.

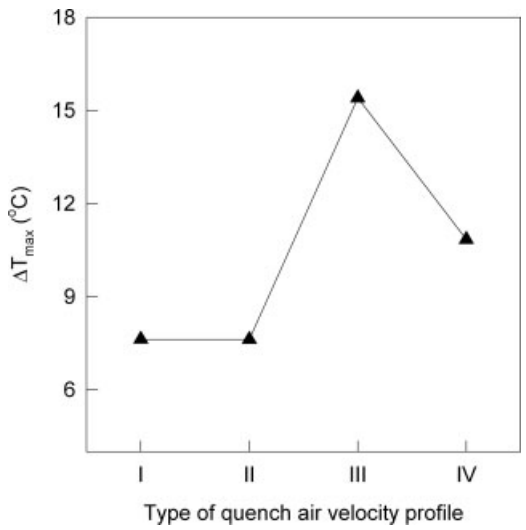

Figure 8 Maximum temperature difference for different quench air profiles: simulation condition, No. 2.

air velocity profile at initial deformation zone leads to a decrease in maximum temperature difference between the core and surface.

References

1. Matsui, M. Sen-I Kikai Gakkaishi 1981, 34, 319.
2. Takeda, T. Sen-I Gakkaishi 1992, 48, 405.
3. Nakajima, T.; Kajiwara, K.; Mclntyre, J. E. Advanced Fiber Spinning Technology; Woodhead: Cambridge, 1994.
4. Park, C. W. AIChE J 1990, 36, 2.
5. Kikutani,. T.; Radhakrishnan, J.; Arikawa, S.; Takaku, A.; Okui, N.; Jin, X.; Niwa, F.; Kudo, Y. J Appl Polym Sci 1996, 62, 1913.
6. Lee, W. S.; Park, C. W. J Appl Mech 1995, 62, 511.
7. Hutchenson, K. W.; Edie, D. D.; Riggs, D. M. J Appl Polym Sci 1984, 29, 3621.
8. Bell, W. P.; Edie, D. D. J Appl Polym Sci 1987, 33, 1073.
9. Chung, B. T. F.; Iyer, V. J Appl Polym Sci 1992, 44, 663.
10. Shimizu, J.; Okui, N.; Kikutani, T.; High-Speed Fiber Spinning; Wiley Interscience: New York, 1985; p 173.
11. George, H. H.; Holt, A.; Buckley, A. Polym Eng Sci 1980, 23, 95.
12. Dutta, A.; Nadkarni, V. M. Tex Res J 1984, 54, 778.
13. Matsuo, T. J Appl Polym Sci 1976, 20, 367.
14. Dutta, A.; Nadkarni, V. M. Tex Res J 1984, 54, 35.
15. Kase, S.; Matsuo, T. J Polym Sci 1965, 3, 2541.
16. Ishibash, T.; Aoki, K.; Ishii, T. J Appl Polym Sci 1970, 14, 1597.